The Effect of Hydrostatic Pressure on Protein Crystals Investigated by Molecular Simulation

DARRIN M. YORK,[1,2]* TOM A. DARDEN[4] and LEE G. PEDERSEN[3,4]
[1]*Department of Chemistry, Duke University, Durham, NC 27706, U.S.A.*
[2]*North Carolina Supercomputing Center, a Division of MCNC, RTP, NC 27709-12889, U.S.A.*
[3]*Department of Chemistry, University of North Carolina, Chapel Hill, NC 27599-3290, U.S.A.*
[4]*National Institute of Environmental Health Sciences, Research Triangle Park, NC 27709, U.S.A.*

Abstract. The effect of hydrostatic pressure on protein crystal structures is examined with molecular simulation. Four 1 ns molecular dynamics simulations of bovine pancreatic trypsin inhibitor in a crystal unit cell have been performed at solvent densities corresponding to 32%, 36%, 40%, and 44% solvent. Electrostatic interactions in the crystalline environment were treated rigorously with Ewald sums. The effect of varying the solvent density at constant unit cell volume is analyzed with respect to changes in protein structure, atomic fluctuations, solvation, and crystal packing. The results indicate the solvent density range 36–40% gives excellent overall agreement with high resolution crystallographic data (~0.3 Å rms backbone deviation). The low density (32%) and high density (44%) simulations have larger deviations.

Key words: Crystal, Ewald, molecular dynamics, pressure, protein, simulation.

Introduction

The majority of experimental structural information for biological macromolecules to date has been provided by X-ray crystallography. There is considerable evidence that protein structure generally is not significantly altered upon crystallization [1,2]. Nonetheless, the structure of a protein in a crystalline environment and in solution may be expected to differ [3]. The degree to which this occurs depends on the presence of crystal packing contacts, and changes in solvation. Typically, protein crystals contain between 30% and 70% solvent by volume [1]. However, solvent contents may vary, being as high as 90% or as low as 25% [2]. It is therefore of interest to understand the effect of solvent content on the crystal packing and solvation of protein crystal structures.

Crystal packing and solvation may be attenuated by external variables such as ion concentration, pH, temperature, and pressure. Here, we focus on the latter. Pressure induced effects on protein structure and solvation have been studied by a variety of experimental techniques [4]. It is known, for example, that pressure can induce denaturation [5] and cause changes in secondary structure [6]. Recently, the effect of hydrostatic pressure on the structure [7] and solvation [8] of hen egg-white lysozyme at 1 atm and 1000 atm has been studied by X-ray crystallography.

Molecular dynamics (MD) simulations provide a useful tool for probing the effect of environment on protein structure. Several studies have been reported that examine the effect of solvation on protein structure by directly comparing

*Author for correspondence.

A. Pullman et al. (eds.), Modelling of Biomolecular Structures and Mechanisms, 203–215.

molecular dynamics simulations in a crystalline environment to those in solution [9–12]. There are several compelling reasons why crystal simulations are of interest. The abundance of X-ray crystal structures provides a wealth of experimental structural data that frequently are used as starting points for theoretical investigations. Consequently, crystal simulations can be used to assess the reliability of simulation force fields and methodologies by direct comparison to accurate experimental data. Moreover, unlike solution simulations, the boundary conditions of a crystal are well defined. Recent simulation studies of protein crystals indicate accuracy comparable to that observed between different crystallographic forms can be obtained by proper treatment of long-range electrostatic interactions [York *et al.* (1994) *Proc. Natl. Acad. Sci. USA* **91**, 8715].

In this study, we examine the effect of variations in pressure on the structure of bovine pancreatic trypsin inhibitor (BPTI) in a crystalline environment using molecular dynamics. The form I crystal of BPTI has been determined by X-ray crystallography [13], and subsequently this protein has been the focus of a number of theoretical investigations (for review see Reference 14). Recently two studies have investigated the effect of pressure on the structure of BPTI in solution [15,16]. However, to our knowledge, the effect of pressure on a protein crystal has not been studied by molecular simulation. Herein we examine the effect of variations in solvent density (and hence pressure) at constant unit cell volume on the structure, atomic fluctuations, solvation, and crystal packing of BPTI. We demonstrate that with appropriate solvent density, excellent agreement with high resolution crystallographic data can be obtalned (~0.3 Å deviation), whereas elevated or reduced density leads to greater deviation.

Methods

We have performed four 1-ns molecular dynamics simulations of BPTI in a crystal unit cell with variable solvent density. The crystalline environment modeled in this study was that of the form I crystal reported by Diesenhofer and Steigman [13] (space group $P2_12_12_1$, $a = 43.1$ Å, $b = 22.9$ Å, $c = 48.6$ Å). The unit cell contains four protein molecules and 240 crystallographic waters (60 per protein molecule). The net charge of each protein molecule was taken to be +6 corresponding to the normal protonation state of the component amino acids at neutral pH. Twenty four chloride counterions were added to neutralize the system. Water molecules were packed in the interstitial space between protein molecules at four different densities. The resulting crystalline systems contained a total of 492, 552, 612, and 672 water molecules, corresponding to approximately 32%, 36%, 40%, and 44% solvent by volume. The form I crystals have been estimated experimentally to be approximately 36% solvent [17]; however, no density measurements have been reported.

Molecular mechanics and dynamics calculations were performed using a modified version of the AMBER3.0 software package. The all-atom force field [18] was employed for protein molecules, and water was treated using the TIP3P model [19]. Chloride ion parameters were taken from Lybrand *et al.* [20] ($r_0 = 2.495$ Å, $\epsilon = 0.107$ kcal/mol). Covalent bonds involving hydrogen were constrained using a modified SHAKE algorithm [21].

Electrostatic forces in the crystal were treated using the Ewald summation convention calculated using the Particle-Mesh Ewald technique [22]. The external dielectric was taken to be infinite so that the surface term in the Ewald expression vanishes. Rigorous treatment of long-range electrostatic forces in this way has been demonstrated to be necessary for proper behavior in simulations of large protein crystals [12,23].

The crystallographic structure provided the unrefined geometry of the protein heavy atoms and structural waters. Hydrogens were added using the internal geometries in the AMBER database, followed by conjugate gradient energy minimization keeping the heavy atom positions fixed. Bulk water molecules were initially packed in the unit cell to low density (32%), energy minimized, and equilibrated with 100 ps of MD keeping the solute (heavy atoms and minimized hydrogens) fixed. Chloride ions were added as follows. The potential at each bulk water oxygen position was evaluated, and the 24 water molecules with the most favorable electrostatic potentials were replaced by chloride ions. The resulting (low density) system was then re-equilibrated with constrained energy minimization and molecular dynamics. Higher density systems were constructed by periodically checking the solvent bath for cavities (1.4 Å radius) during equilibration, and packing the cavities with additional waters. Once fully packed, each higher density system (36%, 40%, 44%) was equilibrated in the same manner as the low density (32%) system. The equilibrated systems were relaxed with 200 steps unconstrained energy minimization to arrive at the starting configurations for full MD. Initial velocities were obtained from a Maxwellian distribution at 1 K, and integration was performed using a 1 fs time step. Systems were initially heated to 298 K over 10 ps by coupling to a thermal bath (temperature relaxation time 0.4 ps). Molecular dynamics was carried out at constant temperature and volume to 1 ns with coordinate files output every 0.5 ps.

Results and Discussion

Here we give a preliminary account of the overall changes in structure and atomic motions predicted for a protein crystal at variable solvent densities. A more thorough study, particularly of the details of the protein-water interactions, is forthcoming.

(i) ROOT-MEAN-SQUARE POSITIONAL DEVIATIONS

The deviation in structure of the simulated protein molecules from the crystallographic structure can be monitored by the root-mean-square positional deviation (rmsPD). The rmsPD of one structure relative to another is obtained by optimal superposition (in a least squares sense) of a set of topologically equivalent atoms [24]. Typically, atom sets consisting of backbone atoms —(N—C_α—C)—, or all heavy (non-hydrogen) atoms, are chosen for the least square fit. Recently, the use of atom sets consisting of heavy atoms with relatively low crystallographic temperature factors (<20 $Å^2$) has been recommended for fitting procedures [25].

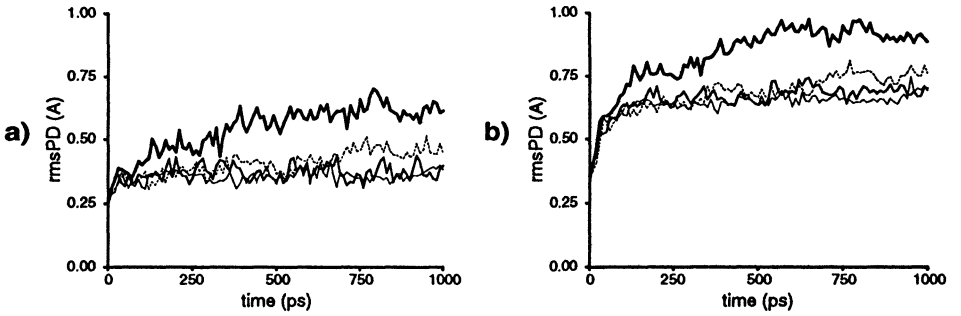

Fig. 1. Time evolution of the root-mean-square positional deviation (rmsPD) of the instantaneous unit cell average (average of the 4 protein monomers at each time point) for (a) backbone (N—C_α—C) atoms, and (b) heavy atoms with crystallographic temperature factors <20 Å^2. Different simulations are indicated by different line styles: 32% (thick solid line), 36% (medium line), 40% (thin solid line), 44% (thin dotted line).

We include the latter convention in this section for comparison. Figure 1(a,b) shows the time evolution of the rmsPD values of the simulated structures relative to the crystallographic structure for each simulation. Equilibration of the rmsPD occurs by 250 ps for the higher density simulations (36%, 40%, and 44%). The low density simulation (32%) requires slightly longer (~400 ps). The asymptotic values of the rmsPD for backbone atoms (32%, 36%, 40%, 44%: 0.61, 0.38, 0.36, 0.42 Å, respectively) and heavy atoms (0.92, 0.68, 0.65, 0.71 Å, respectively) are quite small relative to earlier MD simulations of proteins of comparable size [25]. The stability of the rmsPD values over the relatively long simulation period (1 ns) suggests the structures are equilibrated within a local region of configuration space.

(ii) AVERAGE STRUCTURES

Crystallographic structures represent a time average of an ensemble of protein molecules in a crystal lattice. The fundamental (periodic) repeating unit of the crystal is the unit cell. However, within the unit cell, there can be several structurally equivalent asymmetric units that are related by crystallographic symmetry. In the case of form I crystals of BPTI, the asymmetric unit consists of a single protein molecule. The simulation average structure should therefore include contributions from all of the protein molecules at each time point. The average structure can be obtained by transforming each of the protein molecules to a common local reference frame by applying the inverse $P2_12_12_1$ symmetry operations at each time point. The sampling distribution used to obtain the average involves the 'ensemble' of $M = 4$ transformed protein structures at each time point. The total number of structures in the distribution is $M \times N$ where N is the number of time points and M is the number of protein molecules (asymmetric units) in the unit cell. We denote quantities derived from this distribution by the prefix *cell-* (e.g. *cell*-average, *cell*-variance). Alternately, if we are interested in the statistical behavior of individual molecules, a distribution for each molecule can be constructed involving

TABLE I

Comparison of the rmsPD (Å) of the *cell*-average and *time*-average structures (0.25 to 1 ns) from the X-ray crystal structure

	Simulation			
Structure/atom set	32%	36%	40%	44%
cell-average structures				
backbone[a]	0.54	0.33	0.31	0.39
heavy atom[b]	0.84	0.63	0.60	0.67
time-average structures[c]				
backbone[a]				
M_1	1.09	0.46	0.31	0.45
M_2	0.41	0.36	0.35	0.37
M_3	1.16	0.33	0.36	0.40
M_4	0.38	0.35	0.39	0.42
heavy atom[b]				
M_1	1.40	0.77	0.64	0.76
M_2	0.72	0.68	0.69	0.67
M_3	1.45	0.62	0.64	0.71
M_4	0.75	0.69	0.67	0.73

[a]Main chain N—Cα—C atoms (174 total).
[b]All heavy (non-hydrogen) atoms (454 total).
[c]Monomers 1–4 are designated $M_1, \ldots, M_4$.

only sampling in time, denoted by the prefix *time-* (e.g. *time*-average, *time*-variance).

Table I compares the rmsPD of the simulation *cell*-average and *time*-average structures with respect to the crystallographic structure. Atomic positions from the trajectories were sampled every 0.5 ps from 0.25 to 1 ns. The average structure from the 40% simulation has the lowest rmsPD (0.31 Å backbone), whereas the average structure from the 32% simulation has the largest rmsPD (0.54 Å backbone). The 36% and 40% structures are remarkably similar to each other [rmsPD 0.12 Å (backbone) and 0.23 Å (all heavy atoms)]. This is consistent with observations that the 1 atm and 1000 atm crystal structures of egg-white lysozyme have rmsPD values of 0.12 Å (main-chain N, C_α, C_β, C, O atoms) and 0.20 Å (all heavy-atoms) [7]. Figure 2 shows the rmsPD values of the *cell*-average structures as a function of alpha carbon. The main deviations in the 32% structure occur at the protein termini, and at residues 12 and 36. The latter are flexible glycine residues that are not involved in secondary structure. Peaks in the alpha carbon rmsPD observed in all the *cell*-average structures occur at residues Ala^{25} and Gly^{28}. These residues correspond to the first and last residues of a four-residue hydrogen bonded turn separating β-strands in an antiparallel sheet (see below).

(iii) GLOBAL STRUCTURAL PROPERTIES

Changes in the overall shape of the protein structures are reflected by global structural properties such as the radius of gyration and solvent accessible surface area (Table II). The radius of gyration shows a slight monotonic decrease with

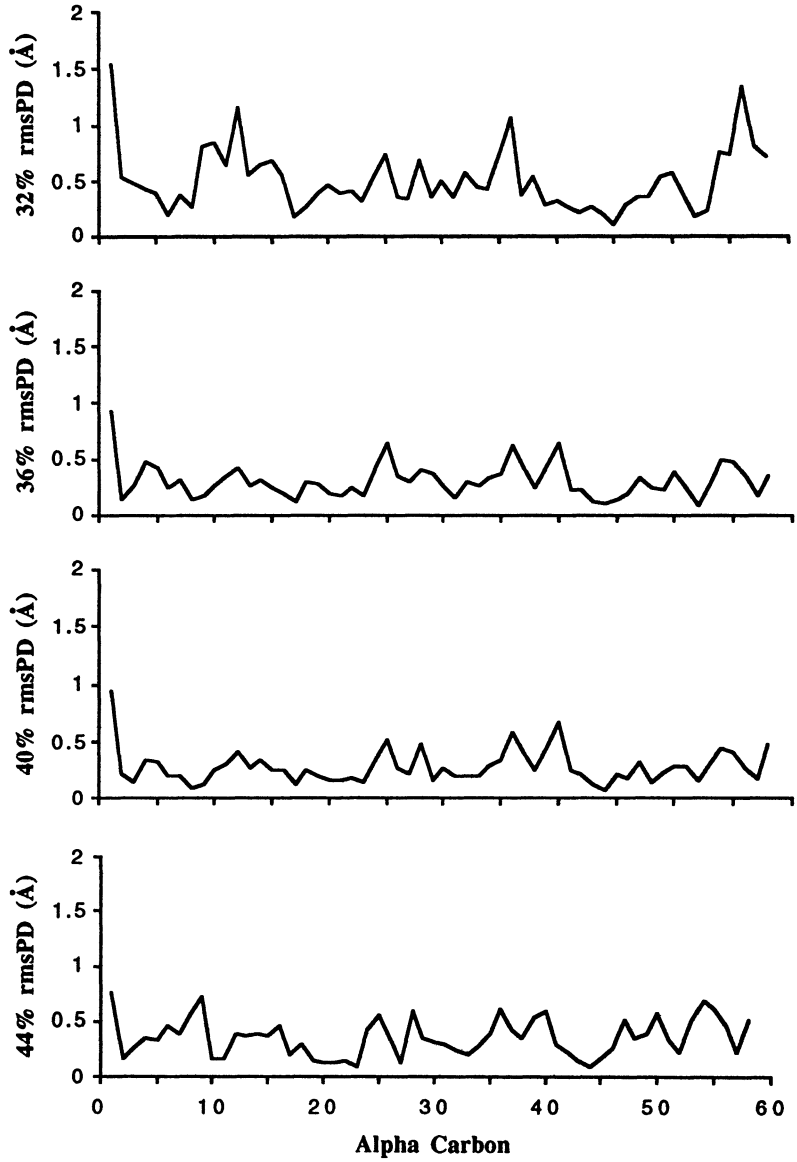

Fig. 2. Comparison of the rmsPD of the *cell*-average structures (0.25–1 ns) from the X-ray structure as a function of alpha carbon.

increasing solvent density (10.93–10.85). The values are all slightly smaller than for the crystallographic structure by about 1 percent. The radius of gyration can be represented as a vector quantity by its principal components (Rg_x, Rg_y, Rg_z). The deviation in the shape of the simulated *cell*-average structures from the crystallographic structure can be measured by taking the norm of the difference of the principle components (*dev. Rg* in Table II). The deviation of the radius of

TABLE II

Radius of gyration and solvent accessible surface area of the *cell*-average structures $\langle \cdots \rangle_{cell}$ and X-ray crystal structure

	Structure				
Property	$\langle 32\% \rangle_{cell}$	$\langle 36\% \rangle_{cell}$	$\langle 40\% \rangle_{cell}$	$\langle 44\% \rangle_{cell}$	X-ray[a]
Rg[b]	10.93	10.91	10.89	10.85	11.0
Rg_x	8.39	8.42	8.43	8.39	8.59
Rg_y	5.41	5.32	5.29	5.30	5.24
Rg_z	4.46	4.44	4.43	4.38	4.44
dev. Rg[c]	0.26	0.19	0.17	0.22	
Surface area[d]	4151	4178	4214	4184	4279

[a]X-ray structure with minimized AMBER hydrogens.
[b]Radius of gyration Rg (Å); the three principle components are designated (Rg_x, Rg_y, Rg_z).
[c]Deviation in the radius of gyration of the simulation average structures relative to the X-ray structure computed as the norm of the difference of the principle components.
[d]Solvent accessible surface area (Å^2) calculated using the program DSSP [24].

gyration is smallest for the 40% *cell*-average structure (0.17 Å) indicating the globular shape is more similar to the crystallographic structure than that of the other *cell*-average structures. Interestingly, the solvent accessible surface area does not show the same monotonic behavior with solvent density as the radius of gyration, but has a maximum at the 40% structure (4214 Å^2) where it is closest to the crystallographic value (4279 Å^2).

(iv) ATOMIC FLUCTUATIONS

Atomic fluctuations give information about the motion of atoms vibrating in a local potential of mean force. The root-mean-square positional fluctuations (rmsPF) can be measured directly from the MD simulations using either the *cell*-variance or the *time*-variances (Figure 3). Atomic fluctuations can be estimated from the crystallographic B values through the equation $\langle \Delta \mathbf{r}_i^2 \rangle^{1/2} = (3B_i/8\pi^2)^{1/2}$, where $\langle \Delta \mathbf{r}_i^2 \rangle^{1/2}$ is the rmsPF of atom i, and B_i is the corresponding B-value [27]. The absolute values of the fluctuations derived from the crystallographic data contain additional contributions such as lattice disorder that are not present in the MD simulations. Consequently, the absolute values of the experimentally derived fluctuations are less reliable than are their relative values [28]. In way of comparison, it is useful to compute the Pearson's correlation coefficient between the simulated and experimentally derived fluctuations. Table III shows the average backbone and side-chain heavy atom atomic fluctuations determined from the simulation *time*-variances and *cell*-variance, and estimated from the crystallographic B values. In all cases, the correlation coefficient was in the range 0.5–0.7. The average fluctuations decrease considerably from the 32% to the 44% simulation. This is consistent with the intuitive argument that, within some range, the pressure effect would tend to damp atomic fluctuations in the protein. In contrast, the fluctuations from the 36% and 40% simulations are almost identical. It is probable that the 36–40% solvent density range closely resembles that of the native crystal, and

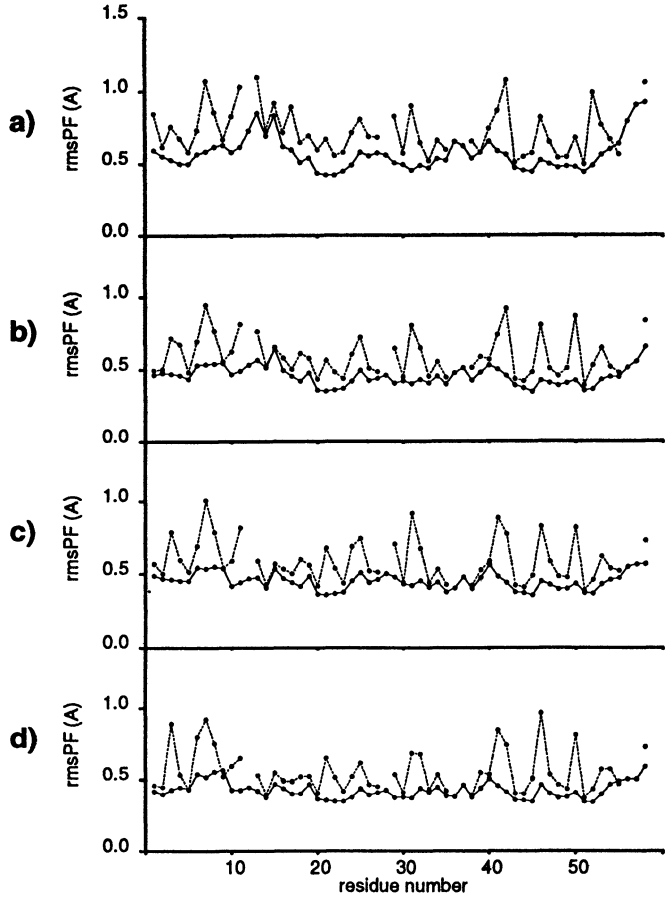

Fig. 3. Comparison of the rmsPF (0.25–1 ns) for main-chain heavy atoms (N—Cα—CO) (solid lines) and side-chain heavy atoms (dotted line) for the simulations: (a) 32%, (b) 36%, (c) 40%, and (d) 44%.

hence one might expect the structure and fluctuations to be stable in this range. Similarly, a minor decrease in the average experimental *B*-factors (1 Å^2) was observed in the 1000 atm crystal structure of lysozyme, corresponding to a difference of approximately 0.04 Å rmsPF [7].

(v) SECONDARY STRUCTURE

Secondary structure reflects the nature of intramolecular hydrogen bonding. Remarkably, the secondary structural assignments for the 36%, 40%, and 44% *cell*-average structures are identical to those of the crystallographic structure (Table IV). In contrast, the 32% *cell*-average structure has deviations in secondary structure at residues 3–6, 43, and 56. The latter two involve residues in loops or turns. The most striking feature of the 32% *cell*-average structure is that residues 3–6

TABLE III

Simulated and experimentally derived root-mean-square positional fluctuations (Å) in the BPTI form I crystal. Average simulated fluctuations derived from the *time*-variances and *cell*-variance (see text) are shown. The correlation coefficients for the simulation results with the experimental results are given in parentheses

	Simulation				
distribution/atom set	32%	36%	40%	44%	X-ray
cell-distribution					
backbone[a]	0.57 (0.7)	0.45 (0.6)	0.45 (0.6)	0.42 (0.5)	0.68
sidechain[b]	0.73 (0.7)	0.60 (0.7)	0.60 (0.7)	0.57 (0.6)	0.78
time-distribution[c]					
backbone[a]	0.95 (0.5)	0.55 (0.5)	0.55 (0.5)	0.46 (0.5)	0.68
sidechain[b]	1.15 (0.6)	0.72 (0.7)	0.71 (0.7)	0.64 (0.7)	0.78

[a]Main-chain N—Cα—CO atoms (232 total).
[b]Heavy (non-hydrogen) side-chain atoms (222 total).
[c]Atomic fluctuations were computed from the *time*-distributions for each protein monomer and then averaged over the four monomers.

TABLE IV

Secondary structural assignments for the simulation *cell*-average structures and crystallographic structure in the BPTI form I crystal

Structure	Secondary Structural Assignment[a]

	RPDFCLEPPYTGPCKARIIRYFYNAKAGLCQTVYGGCRAKRNNFKSAEDCMRTCGGA[b]					
	1	2	3	4	5	
	12345678901234567	8901234567890123456789012345	6789	01	2345678	01234567 8
X-ray	GGGGS	S	EEEEEEETTTTEEEEEEE	SSS	SS	BSSHHHHHHHS
32%	HHHHS	S	EEEEEEETTTTEEEEEEE	SSS	S	BSSHHHHHHHT
36%	GGGGS	S	EEEEEEETTTTEEEEEEE	SSS	SS	BSSHHHHHHHS
40%	GGGGS	S	EEEEEEETTTTEEEEEEE	SSS	SS	BSSHHHHHHHS
44%	GGGGS	S	EEEEEEETTTTEEEEEEE	SSS	SS	BSSHHHHHHHS

[a]Secondary structural assignments were made using the program DSSP [24]: H = α-helix, G = 3_{10}-helix, E = β-sheet, T = hydrogen bonded turn, S = bend, B = isolated β-bridge.
[b]BPTI amino acid sequence.

have converted from the 3_{10}-helix to an α-helix. This is consistent with theoretical studies that suggest a relatively low barrier for the $3_{10} \leftrightarrow \alpha$-helix transition (0.2 kcal/mol), with the α-helical form favored by aqueous conditions [29].

BPTI contains an interesting aromatic hydrogen bonding interaction between residues Gly^{37}----Tyr^{35}----Asn^{44}. The backbone NH of Gly^{37} and the side-chain NH2 of Asn^{44} are hydrogen bond donors on opposite sides of the aromatic Tyr^{35} ring. This delicate interaction is necessary for preserving the native structure since the Y35G mutant crystal structure has significant deviation in this region [32]. The aromatic hydrogen bond interaction is maintained in the 36%, 40%, and 44% simulations; however, in the 32% simulation it is significantly weakened. An

TABLE V
Intermolecular hydrogen bond (heavy atom–heavy atom) distances in BPTI crystal form I[a]

H-bond X—H---Y		X–Y distance (Å)				
donor (X)	acceptor (Y)	X-ray	$\langle 32\% \rangle_{cell}$	$\langle 36\% \rangle_{cell}$	$\langle 40\% \rangle_{cell}$	$\langle 44 \rangle_{cell}$
Asp^{3} N	Glu^{49} OE1	3.07	**3.65**	3.38	3.16	3.04
Arg^{17} NE	Lys^{26} O	2.97	3.12	2.76	2.74	2.74
Arg^{17} NH-1	Ala^{58} O	–	3.33	2.76	2.65	2.70
Arg^{17} NH-2	Ala^{58} O	2.95	3.35	3.13	3.42	3.25
Arg^{17} NH-1	Ala^{58} OXT	–	–	3.13	3.37	3.17
Arg^{17} NH-2	Ala^{58} OXT	2.67	**3.42**	2.73	2.66	2.70
Arg^{39} NH-1	Tyr^{21} OH	2.70	**3.45**	3.30	**3.76**	**3.84**
Arg^{39} NE	Glu^{49} OE-1	3.04	2.66	2.69	2.71	2.73
Arg^{39} NH-2	Glu^{49} OE-2	2.80	3.00	2.69	2.71	2.70
Arg^{42} NH-1	Tyr^{10} OH	3.26	–	**3.88**	3.50	**3.98**
Arg^{42} NH-1	Arg^{39} O	3.28	–	–	–	–
Ala^{48} N	Arg^{39} NH-2	3.34	3.70	3.67	3.65	3.74

[a]Donor–acceptor heavy-atom–heavy-atom distances less 4 Å are shown. Distances shown in **bold** differ from the crystallographic values by more than 0.5 Å.

extensive discussion of intramolecular hydrogen bonding in BPTI is given in References 17, 30, and 31.

(vi) INTERMOLECULAR HYDROGEN BONDING

The crystal structure of BPTI (form I) contains several intermolecular hydrogen bonds that stabilize the protein molecules in the crystal lattice [13]. An interesting question arises as to whether the crystal packing environment is disrupted by variations in hydrostatic pressure. Table V compares the intermolecular hydrogen bond donor–acceptor distances for the crystallographic and *cell*-average structures. There are ten intermolecular hydrogen bonds present in the crystallographic structure. Of these ten, five are preserved in the 32% simulation (where 'preserved' is defined as having a distance deviation of less than 0.5 Å from the crystallographic result), eight are preserved in the 36% and 40% simulations, and seven are preserved in the 44% simulation. In all of the simulations the interaction between Arg^{39} and Arg^{42} was absent, and the interaction between Arg^{39} and Tyr^{21} was significantly reduced. We conclude that the crystal packing environment is sensitive to pressure. For an extensive discussion of intermolecular hydrogen bonding in BPTI crystal structures see Reference 30.

(vii) SOLVENT MOBILITY

Protein crystals generally contain solvent molecules (water and ions) that are structurally 'bound' to the protein molecules in addition to bulk-like solvent in the interstitial spaces. The mobility of the solvent might be expected to change

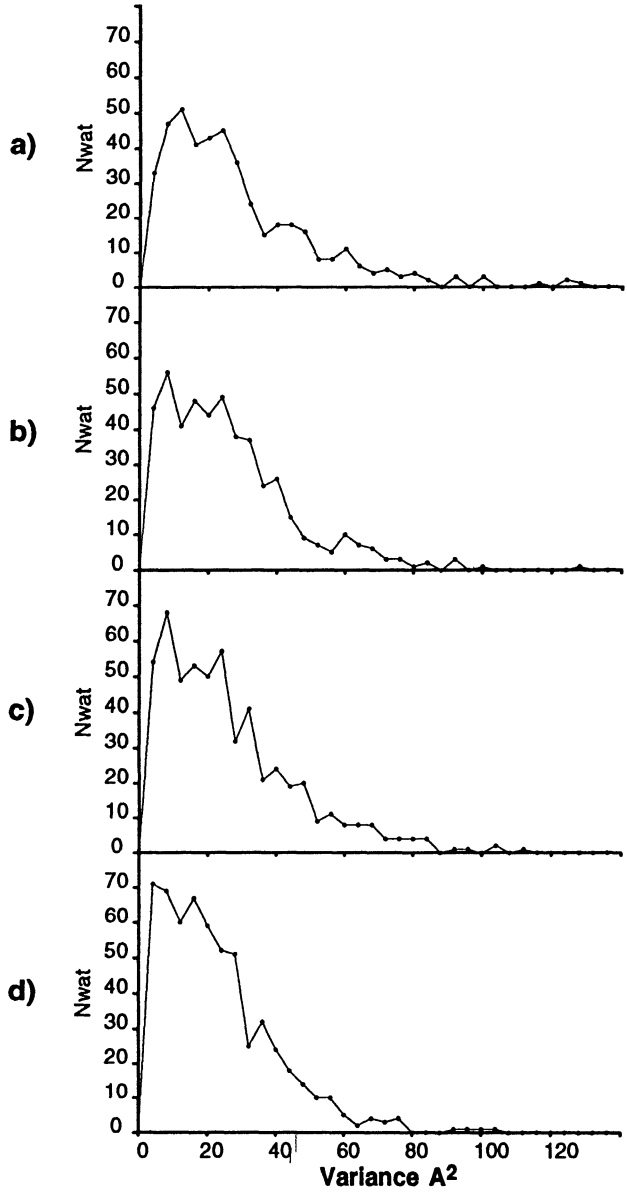

Fig. 4. Histograms of the water molecule variance (0.25–1 ns) in the simulations: (a) 32%, (b) 36%, (c) 40%, and (d) 44%.

with variation in pressure. The average water and chloride ion variance (0.25–1 ns) is largest in the low density (32%) simulation (25.7, 9.4 $Å^2$, respectively) and smallest in the high density (44%) simulation (20.2, 6.5 $Å^2$). Surprisingly, the 36% simulation has slightly smaller water and chloride ion variances (22.7, 6.6 $Å^2$) than the 40% simulation (23.9, 7.1 $Å^2$). Hence, there appears to be an inflexion in the

average solvent mobility as a function of pressure in the density range 36–40%. This compares with the results of the 1 atm and 1000 atm crystal structures of egg-white lysozyme that indicate fluctuations in the structural solvent are relatively insensitive to pressure as indicated by the B factors [8]. In all of the simulations, the variance of the water molecules was approximately three times greater than the variance of the chloride ions. The relatively large variance (related to the diffusion constant) for the TIP3P water has been previously noted [14]. Histograms showing the distribution of water molecule variance in the simulations are shown in Figure 4. The general trend as the solvent density increases is that of a slight shift in the distribution towards lower variances.

Conclusion

Simulations of BPTI in a crystal unit cell (form I) have been carried out to 1 ns at solvent densities corresponding to approximately 32%, 36%, 40%, and 44% solvent by volume. The solvent content estimated for the native crystal structure is in the range of 36–40%. Results of the 36% and 40% simulations demonstrate that the protein structure, atomic fluctuations, and crystal packing environment are stable in this range, and agree well with crystallographic data (average structures give rms backbone deviations of ~0.3 Å from the native crystal structure). The 40% simulation gives the best overall agreement with experimental data. The 32% and 44% simulations show more substantial deviations in structure, particularly the low density (32%) simulation. Atomic fluctuations are considerably exaggerated in the 32% simulation, and damped in the 44% simulation relative to the stable fluctuations observed for the 36% and 40% simulations. Crystal packing is also disrupted in the 32% and 44% simulations. The average variance of the solvent and counterions as a function of solvent density (pressure) has an inflexion in the 36–40% solvent density range. The results reported here represent the first study of the effects of hydrostatic pressure on large protein crystals using molecular simulation.

Acknowledgement

DY acknowledges the National Science Foundation for a postdoctoral fellowship jointly funded by the North Carolina Supercomputing Center, MCNC, RTP, NC. This work was supported by grants from NIEHS (LP,TD). Supercomputing time was provided by the Biomedical Supercomputing Center, National Cancer Institute, FCRDC, the Pittsburgh Supercomputing Center, Pittsburgh, PA, and the North Carolina Supercomputing Center, RTP, NC.

References

1. B. Matthews: in H. Neurath and R. Hill, Eds., *The Proteins*, *3rd ed.*, *Vol. 3*, Academic Press, New York, p. 403 (1977).
2. T. Creighton: in *Proteins*, *2nd ed.*, W. H. Freeman & Co., New York (1993).
3. A. Bax: *Ann. Rev. Biochem.* **58**, 223 (1989).

4. G. Weber: in R. van Eldik and J. Jonas, Eds.: *High Pressure Chemistry and Biochemistry*, D. Reidel Publishing Company, Boston (1986).
5. P. Wong and K. Heremans: *Biochim. Biophys. Acta.* **956**, 1 (1988).
6. D. Carrier, H. Mantsch, and P. Wong: *Biopolymers* **29**, 837 (1990).
7. C. Kundrot and F. Richards: *J. Mol. Biol.* **193**, 157 (1987).
8. C. Kundrot and F. Richards: *J. Mol. Biol.* **200**, 401 (1988).
9. W. F. van Gunsteren and M. Karplus: *Biochemistry* **21**, 2259 (1982).
10. W. F. van Gunsteren and H. J. C. Berendsen: *J. Mol. Biol.* **176**, 559 (1984).
11. P. Krüger, W. Strassburger, A. Woller, and W. F. van Gunsteren: *Eur. Biophys. J.* **13**, 77 (1985).
12. D. York, T. Darden, L. Pedersen, and M. Anderson: *Biochemistry* **32**, 1443 (1993).
13. J. Deisenhofer and W. Steigmann: *Acta Crystallogr. B* **31**, 238 (1975).
14. V. Daggett and M. Levitt: *Ann. Rev. Biophys. Biomol. Struct.* **22**, 353 (1993).
15. D. Kitchen, L. Reed, and R. Levy: *Biochemistry* **31**, 10083 (1992).
16. R. Brunne and W. van Gunsteren: *FEBS Lett.* **323**, 215 (1993).
17. A. Wlodawer, J. Walter, R. Huber, and L. Sjölin: *J. Mol. Biol.* **180**, 301 (1984).
18. S. J. Weiner and P. A. Kollman: *J. Comp. Chem.* **7**, 230 (1986).
19. W. L. Jorgensen, J. Chandrasekhar, J. D. Madura, R. W. Impey, and M. Klein: *J. Chem. Phys.* **79**, 926 (1983).
20. T. Lybrand, J. McCammon, and G. Wipff: *Proc. Natl. Acad. Sci. USA* **83**, 833 (1986).
21. J. Ryckaert, G. Ciccotti, and H. Berendsen: *J. Comput. Phys.* **23**, 327 (1977).
22. T. Darden, D. York, and L. Pedersen: *J. Chem. Phys.* **98**, 10089 (1993).
23. D. York, T. Darden, and L. Pedersen: *J. Chem. Phys.* **99** 8345 (1993).
24. A. D. McLachlan: *J. Mol. Biol.* **128**, 49 (1979).
25. D. Kitson, F. Avbelj, J. Moult, D. Nguyen, J. Mertz, D. Hadzi, and A. Hagler: *Proc. Natl. Acad. Sci. USA* **90**, 8920 (1993).
26. W. Kabsch and C. Sander: *Biopolymers* **22**, 2577 (1983).
27. M. Karplus and G. Petsko: *Nature* **347**, 631 (1990).
28. G. Petsko and D. Ringe: *Ann. Rev. Biophys. Bioeng.* **13**, 331 (1984).
29. M. Smythe, S. Huston, and G. Marshall: *J. Am. Chem. Soc.* **115**, 11594 (1993).
30. A. Wlodawer, J. Deisenhofer, and R. Huber: *J. Mol. Biol.* **193**, 145 (1987).
31. K. Berndt, P. Güntert, L. Orbons, and K. Wüthrich: *J. Mol. Biol.* **227**, 757 (1992).
32. D. Housset, K-S. Kim, J. Fuchs, C. Woodward, and A. Wlodawer: *J. Mol. Biol.* **220**, 757 (1993).